Article

J. Biol. Regul. Homeost. Agents. 2024; 38(5): 3711–3726
https://doi.org/10.23812/j.biol.regul.homeost.agents.20243805.293

Transcriptome Analyses Identify a Pyroptosis-Related Transcription Factor-microRNA-mRNA Regulatory Network for Vascular Dementia

Qian Yang[1,†], Hui Yang[1,†], Shuai Wang[2], Bi Ma[1,*]

[1]Department of Neurology, The First Affiliated Hospital of Chengdu Medical College, 610500 Chengdu, Sichuan, China
[2]Department of Outpatient, General Hospital of Western Theater Command, 610083 Chengdu, Sichuan, China
*Correspondence: mabi1228@163.com (Bi Ma)
[†]These authors contributed equally.
Published: 1 May 2024

Background: Vascular dementia (VaD) is a kind of cerebrovascular diseases characterized by decreased cognitive function. No effective treatments have been approved for the treatment of VaD. Accumulative evidence reveals that pyroptosis plays a key role in mediating VaD. Therefore, this study aimed to identify pyroptosis-linked hub genes by using bioinformatics analysis and construct a regulatory network among transcription factors (TFs), microRNAs (miRNAs), and mRNAs for VaD.
Methods: Differentially expressed genes (DEGs) in the frontal cortex between VaD and control samples were identified. Several analyses were performed, including functional enrichment, protein-protein interaction (PPI), miRNA-target gene interaction, transcription factor-microRNA (TF-miRNA) interaction, and drug-hub gene interaction. The goal was to obtain pyroptosis-related hub genes and create a TF-miRNA-mRNA regulatory network for VaD.
Results: We identified 27 DEGs related to pyroptosis, nine of which were considered as pyroptosis-related hub genes. These hub genes were nucleotide-binding oligomerization domain-like receptor protein 3 (*NLRP3*), *TLR2*, *CASP1*, heat shock protein 90 kDa alpha family class A member 1 (*HSP90AA1*), *VEGFA*, *AIM2*, *LY96*, *CEBPB*, and *BTK*. In our TF-miRNA-mRNA regulatory network, two hub genes (vascular endothelial growth factor-A (*VEGFA*) and heat shock protein 90 kDa alpha family class A member 1 (*HSP90AA1*)), four miRNAs (*miR-1304-3p*, *miR-1293*, *miR-191-5p*, and *miR-5193*), and five TFs (Early Growth Response Protein 1 (*EGR1*), runt-related transcription factor-1 (*RUNX1*), *SPI1*, PHD finger protein 8 (*PHF8*), and CCAAT/enhancer binding protein beta (*CEBPB*)) were identified as potential biomarkers for VaD. The expression levels of these key target genes, miRNAs, and TFs were verified using an oxygen-glucose deprivation (OGD)-induced SH-SY5Y cell model. The drug-target gene interaction analysis revealed that three drugs (tanespimycin, bevacizumab, and aflibercept) targeting *HSP90AA1* and *VEGFA* could be potential drugs for VaD treatment.
Conclusions: This study built a pyroptosis-related regulatory network among TFs, miRNAs, and target genes for VaD. The results of this study might assist with clarifying the new molecular mechanisms of VaD. Additionally, *HSP90AA1* and *VEGFA* were identified as potential biomarkers or therapeutic targets for VaD treatment.

Keywords: vascular dementia; microRNA; transcription factor; pyroptosis; bioinformatics

Introduction

Vascular dementia (VaD) is a kind of cerebrovascular diseases characterized by impaired cognition, accounting for 20%–30% of dementia cases after Alzheimer's disease (AD) [1]. Although numerous drugs such as cholinesterase inhibitors and memantine have been proposed as potentially efficient in treating VaD, clinical trials indicate that these therapeutic agents have failed to show efficacy in preventing VaD [2]. Unfortunately, with the aging of the world population, the number of individuals affected by aging-related dementia is predicted to triple by 2050, and dementia has emerged as a major public health challenge in this century [3]. Therefore, identifying novel mediators of VaD is currently needed to develop more effective therapeutic strategies targeting VaD.

Pyroptosis, a common form of programmed cell death linked to inflammation, is triggered by the activation of the nucleotide-binding oligomerization domain-like receptor protein 3 (NLRP3) inflammasome. Once activated, NLRP3 activates caspase-1, which in turn induces the cleaving of the pro-interleukin-1beta (pro-IL-1β) and pro-interleukin-18 (pro-IL-18) into IL-1β and IL-18, respectively, and their release. These inflammatory factors can induce cell damage and eventually trigger pyroptosis [4]. Recent evidence suggests that pyroptosis may play a key role in mediating VaD [5–7] and contribute to blood-brain barrier breakdown in diabetes-induced cognitive decline [6]. Inhibition

Journal of
BIOLOGICAL REGULATORS
and Homeostatic Agents

of NLRP3 inflammasome with MCC950 has been shown to improve diabetes-mediated cognitive impairment [7]. However, the possible role of pyroptosis in mediating VaD remains unknown.

Dysregulation of various microRNAs (miRNAs) has been implicated in vascular dementia. In humans and rats with VaD, *miRNA-154-5p* up-regulation was found to be associated with impaired endothelial progenitor cell functions and angiogenesis in VaD rats [8]. In VaD mice, *miR-132-3p* down-regulation was reported, and the infusion of mesenchymal stromal cells-derived exosomal *miR-132-3p* improved synaptic injury and cognitive decline in VaD mice [9]. Dysregulated miRNAs were believed to impair the blood-brain barrier and promote neuronal apoptosis and inflammation, all of which contributed to the development of VaD [10]. However, the functional implications of various miRNAs in regulating pyroptosis in VaD are not fully elucidated.

In this study, the microarray profiles of VaD brain samples from the Gene Expression Omnibus (GEO) were analyzed to identify the pyroptosis-related differentially expressed genes (Pyro-DEGs) between VaD and control. Functional enrichment analyses of the Pyro-DEGs were carried out to examine potential signaling pathways associated with VaD. Protein-protein interaction (PPI) network was built to screen hub Pyro-DEGs. Furthermore, miRNA-hub Pyro-DEG and transcription factor-microRNA (TF-miRNA) interaction analyses were performed to identify the potential transcriptional regulatory factors, and drug-hub Pyro-DEG interaction analysis was used to screen candidate drugs for VaD. The findings of the study might assist with clarifying the new molecular mechanism and therapeutic targets of VaD.

Materials and Methods

The workflow diagram of the present study is presented in Fig. 1.

Identification of Differentially Expressed Genes (DEGs) from Microarray Datasets Associated with VaD

The Gene Expression Omnibus (GEO) (https://www.ncbi.nlm.nih.gov/geo) datasets were searched to obtain two VaD-associated gene expression datasets, GSE122063 (for mRNA analysis) and GSE120584 (for miRNA analysis). The inclusion criteria used to filter VaD-associated datasets included the following: (i) the datasets focused on "Expression profiling by array", (ii) the organism was "homo sapiens", (iii) transcript expression profiles were derived from the samples from both VaD and normal control patients, and (iv) the raw data of the series matrix file(s) can be downloaded for reanalysis. GSE122063 comes from GPL16699 platform. The samples in GSE122063 were derived from human brain frontal cortex tissues of VaD (n = 18) and normal control (n = 22) patients. GSE120584 comes from GPL21263 platform. The blood samples in GSE120584 were obtained from the healthy control (n = 288) and VaD (n = 91) groups.

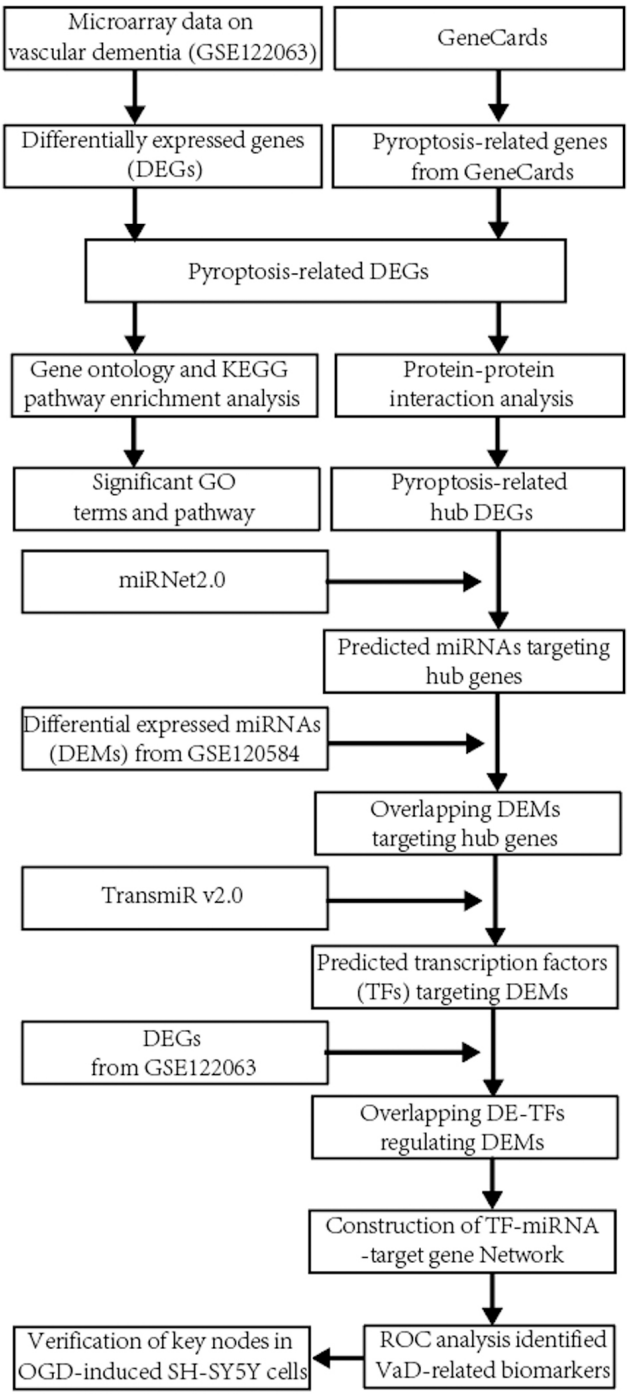

Fig. 1. Workflow diagram of the present study. DEGs, differentially expressed genes; miRNAs, microRNAs; DEMs, differentially expressed miRNAs; KEGG, Kyoto Encyclopedia of Genes and Genomes; VaD, vascular dementia; GO, gene ontology; ROC, receiver operating characteristic.

Differentially Expressed Gene Analysis

The online biological tool Gene Expression Omnibus 2R (GEO2R) (https://www.ncbi.nlm.nih.gov/geo/geo2r/) was applied to screen differentially expressed genes (DEGs) between VaD and control in GSE122063. The *p*-value was modified using the Benjamini and Hochberg method to avoid false positive results. The cut-off criteria of adjusted *p*-value less than 0.05 plus absolute log2 fold change (FC) > 0.585 were set to screen DEGs. The bioinformatics analysis software TBtool (version 1.113, South China Agricultural University, Guangzhou, China) was applied to visualize the volcano plots and heatmaps of DEGs [11].

Identification of Pyroptosis-Related DEGs

The pyroptosis-related genes that were obtained from the online GeneCards dataset (https://www.genecards.org) are presented in **Supplementary Table 1**. Subsequently, to obtain pyroptosis-related differentially expressed genes (Pyro-DEGs), the pyroptosis-related genes were intersected with the total DEGs in GSE122063. TBtool was used to create the Venn diagrams and heatmaps of Pyro-DEGs.

Functional Enrichment Analysis of Pyro-DEGs

Functional enrichment analyses were conducted to investigate the functional role and signaling mechanisms of Pyro-DEGs. The online bioinformatics tool Metascape (https://metascape.org/gp/index.html#/main/step1) was used to perform gene ontology (GO) enrichment and Kyoto Encyclopedia of Genes and Genomes (KEGG) pathway enrichment analysis. The cut-off criteria of an adjusted *p*-value less than 0.05 were statistically significant. Bubble plots of GO and KEGG pathway enrichment analyses of Pyro-DEGs were obtained using the bioinformatics analysis platform SangerBox (http://www.sangerbox.com/) [12].

Creation of Protein-Protein Interaction (PPI) Network and Screening of Hub Genes

To investigate the protein-protein interaction (PPI) among these Pyro-DEGs, the STRING database (http://string-db.org/) was applied to create a PPI network with a cut-off interaction score > 0.4. The interaction result was introduced into Cytoscape software (version v3.8.2, University of California San Diego School of Medicine, San Diego, CA, USA) to identify the top 10 hub genes ranked by high connectivity in this interaction network using the Maximal Clique Centrality (MCC) algorithm. Genes predicted by more than three types of algorithms including MCC, Maximum Neighborhood Component (MNC), and Degree at the same time were considered hub genes for VaD.

Identification of Differentially Expressed miRNAs (DEMs) Targeting Hub Pyro-DEGs and miRNA-Target Gene Regulatory Network Construction

GEO2R was used to identify the DEMs between VaD and control in GSE120584. An adjusted *p*-value less than 0.05 and absolute log2(FC) > 0.5 were set as the cut-off criteria to screen DEMs.

In addition, potential miRNAs that target hub Pyro-DEGS were predicted using miRNet v2.0 (https://www.mirnet.ca/miRNet/home.xhtml), which is a web-based platform that integates four well-known bioinformatics algorithms including miRTarBase v8.0, miRanda, miRecords, and TarBase v8.0. The predicted miRNAs were intersected with the total DEMs in GSE120584 to obtain overlapping DEMs. The overlapping DEMs were filtered based on the following inclusion criteria: the up-regulated DEMs in GSE120584 target the down-regulated Pyro-DEGs in GSE122063, whilst the down-regulated DEMs target the up-regulated Pyro-DEGs. Subsequently, the miRNA-target gene regulatory networks between the overlapping DEMs and their target Pyro-DEGs were constructed and visualized by Cytoscape software (version v3.8.2, University of California San Diego School of Medicine, San Diego, CA, USA).

Identification of Differentially Expressed Transcription Factors (DE-TFs) Targeting DEMs and TF-miRNA Regulatory Network Construction

To investigate the interactions between transcription factors (TFs) and miRNAs, the upstream TFs that target the overlapping DEMs were predicted using the TransmiR v2.0 dataset (http://www.cuilab.cn/transmir) [13]. The predicted upstream TFs were intersected with the total DEGs in GSE122063 to obtain the overlapping DE-TFs. The regulatory networks between the overlapping DE-TFs and their corresponding target miRNAs were created and visualized using Cytoscape software (version v3.8.2, University of California San Diego School of Medicine, San Diego, CA, USA).

Construction of TF-miRNA-Target Gene Regulatory Network

A TF-miRNA-target gene regulatory network was constructed in VaD by combining the miRNA-target gene and TF-miRNA networks and displayed using Cytoscape software (version v3.8.2, University of California San Diego School of Medicine, San Diego, CA, USA). The integrated TF-miRNA-target gene regulatory network was filtered based on the inclusion criteria, which involved discarding the miRNA-target gene pairs that had no predicted regulatory TFs. The topological properties of the regulatory network were analyzed using the NetworkAnalyzer plug-in in Cytoscape software (version v3.8.2,

Journal of
BIOLOGICAL REGULATORS
and Homeostatic Agents

University of California San Diego School of Medicine, San Diego, CA, USA) to identify the key nodes in the network.

Receiver Operating Characteristic (ROC) Curve Analysis

Key TFs and key target genes from GSE122063, and key miRNAs from GSE120584 presented in the TF-miRNA-target gene regulatory network were considered to be potential biomarkers for VaD. The Pyro-DEGs' expression data in GSE122063 were applied to compare the VaD and control groups using MedCalc Statistical Software version 20 (MedCalc Software Ltd., Ostend, Belgium). An independent sample *t*-test was conducted for comparison between groups, and *p* less than 0.05 was considered to be statistically significant. The diagnostic value of these key genes for VaD was evaluated by using ROC analysis. Key target genes and key TFs with the area under the curve (AUC) larger than 0.7 and *p* less than 0.05 were considered potential biomarkers. Key miRNAs with AUC larger than 0.5 and *p* less than 0.05 were identified as potential biomarkers.

Validation of Key Target Genes, miRNAs, and TFs Using Oxygen-Glucose Deprivation (OGD)-Induced SH-SY5Y Cells

To verify the key target genes, miRNAs, and TFs in the regulatory network, an *in vitro* model of cerebral ischemia in human SH-SY5Y neuroblastoma cells were used to examine the detrimental effects of oxygen-glucose deprivation on the gene expression of key nodes. SH-SY5Y cells were purchased from the American Type Culture Collection (cat. no. CRL-22660, Manassas, VA, USA) and maintained in Dulbecco's Modified Eagle's Medium (DMEM)/F-12 complete medium at 37 °C with 5% carbon dioxide (CO_2). Short tandem repeat (STR) characterization was performed at Shanghai Biowing Applied Biotechnology Limited Corporation (Shanghai, China) for cell authentication. Before starting our *in vitro* validation experiments, SH-SY5Y cells were regularly assessed for mycoplasma contamination, and the test results were negative.

SH-SY5Y cells were seeded into a 6-well plate at the density of 5.0×10^5 cells/well and cultured for 24 h. To induce OGD injury [14], the culture medium was replaced with oxygen-glucose-free DMEM, and the SH-SY5Y cells were transferred into an incubator chamber after the oxygen-glucose-free DMEM was produced by bubbling glucose-free DMEM with a gas mixture containing CO_2 and N_2 (5% and 95%, respectively) for 5 min. The chamber was then sealed and flushed with a gas mixture containing 5% CO_2 and 95% N_2 for 5 min at a flow rate of 25 L/min. Finally, the two ports were sealed, and the chamber was placed in an incubator at 37 °C for 24 h to induce lethal OGD. The control cells were cultured in a normoxic condition (95% air and 5% CO_2) with regular DMEM. Immediately after applying OGD, cells were harvested for further analysis.

The mRNA or miRNA expression of key nodes in OGD-induced SH-SY5Y cells were determined using real-time quantitative polymerase chain reaction (RT-qPCR). Total RNA was obtained from cultured SH-SY5Y cells using TRIzol Reagent (cat. no. 15596026, Invitrogen, Carlsbad, CA, USA) following the manufacturer's protocol. 2 µg of RNA was reverse transcribed using SuperScript™ III reverse transcriptase (cat. no. 18010400, ThermoFisher Scientific Inc., Waltham, MA, USA) to synthesize cDNA. The synthesized cDNA was amplified using the SYBR Green Master Mix. The PCR amplification protocol were performed as follows: step 1: initial denaturation at 94 °C for 2 min; step 2: 35 cycles of denaturation at 94 °C for 10 s, annealing at 55–65 °C for 30 s, and extension at 72 °C for 30 s. The primers used in the present study are presented in **Supplementary Table 2**. Glyceraldehyde-3-phosphate dehydrogenase (GAPDH) was used as an intenal reference. Results were normalized to GAPDH expression using the $2^{-\Delta\Delta Ct}$ method. The individual data for RT-qPCR analysis were compared with that of the control group and presented as multiples of the control mean.

For RT-qPCR of miRNAs, total RNA was converted into cDNA using a TaqMan miRNA reverse transcription kit (cat. no. 4366596, Applied Biosystems, Foster City, CA, USA) with specific stem-loop primers. After synthesizing single-stranded cDNA, RT-qPCR amplifications were carried out using an iCycleriQ Real-Time Detection System (version 3.1, Bio-Rad Laboratories, Hercules, CA, USA). The primer used for *miR-1304-3p*, *miR-1293*, *miR-191-5p*, *miR-23a-3p*, *miR-5193*, and *U6* are presented in **Supplementary Table 2**.

Drug-Gene Interaction Analysis

To verify the drug-gene interaction, the Drug-Gene Interaction Database (DGIdb, https://dgidb.genome.wustl.edu/) were explored search for existing drugs that could interact with the hub Pyro-DEGs. Potential drugs that exhibited well-known interaction types with the hub Pyro-DEGs were considered for use in the treatment of VaD. The interactions between the potential drugs and their corresponding target genes were visualized using Cytoscape software version v3.8.2.

Statistical Analysis

The data were subjected to statistical analysis using the SPSS 13.0 statistical package (SPSS Inc., Chicago, IL, USA). An unpaired two-side *t*-test was conducted for comparisons between groups. A *p*-value of less than 0.05 was considered to be statistically significant.

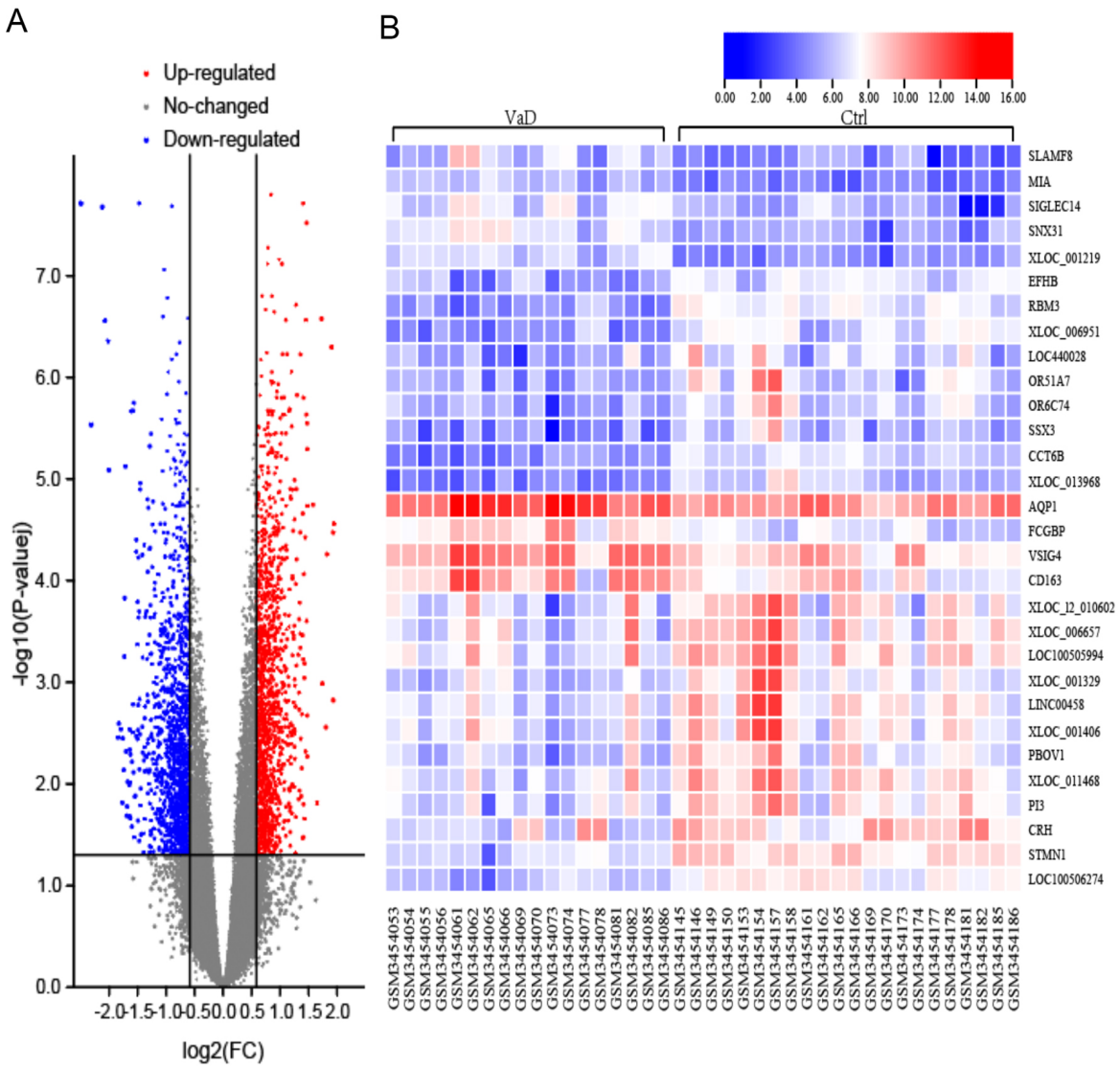

Fig. 2. Identification of differentially expressed genes (DEGs) in VaD. (A) Volcano plot of total DEGs in GSE122063 associated with VaD. (B) Heatmap of the top 30 DEGs in GSE122063. FC, fold change.

Results

Expression Signature of PyroDEGs in GSE122063

First, the online GEO2R tool was applied to screen the differentially expressed genes (DEGs) in brain samples between the VaD patients and corresponding non-dementia controls. Based on the inclusion criteria (adjusted p less than 0.05 and absolute log2(FC) $>$ 0.585), there were a total of 2973 DEGs (1382 up-regulated and 1591 down-regulated) identified and visualized in the volcano plots (Fig. 2A) and heatmap (Fig. 2B) using TBtools. Subsequently, 372 pyroptosis-related genes downloaded from the GeneCards database were intersected with the total DEGs in GSE122063 to obtain a total of 27 pyroptosis-related differentially expressed genes (Pyro-DEGs) (17 up-regulated and 5 down-regulated) (Table 1, Fig. 3).

Functional Enrichment of the Pyro-DEGs in GSE122063

GO enrichment and KEGG pathway analysis were used to deduce the function of the 27 Pyro-DEGs. The results are shown in Fig. 4. For the biological process (BP) category of GO enrichment, the Pyro-DEGs were mainly focused on the inflammatory response, positive regulation of cytokine production, regulation of defense response, etc. (Fig. 4A). The Pyro-DEGs were also focused on the cellular component (CC) category such as membrane raft, membrane microdomain, and vesicle lumen (Fig. 4B). Molecular function (MF) category was focused on the protein domain specific binding, signaling receptor activator activity, and signaling receptor regulator activity (Fig. 4C). KEGG pathway enrichment analysis showed that the Pyro-DEGs were focused on salmonella infection, NOD-like receptor signaling pathway, lipid and atherosclerosis, etc. (Fig. 4D).

Journal of
BIOLOGICAL REGULATORS
and Homeostatic Agents

Table 1. 27 pyroptosis-related DEGs in dataset GSE122063.

Gene.symbol	adj.*p*.Val	Log2(FC)	changes
IKZF1	0.0023	0.895032	up-regulated
BTK	0.00977	0.692539	up-regulated
CD14	0.0112	0.987846	up-regulated
GSDMB	0.00177	0.748021	up-regulated
SIGLEC14	0.00196	1.876486	up-regulated
BST2	0.00588	0.937123	up-regulated
SETD7	0.0000957	–1.14025	down-regulated
TLR2	0.00565	1.29503	up-regulated
VEGFA	0.0268	0.81473	up-regulated
PKN2	0.00802	0.716306	up-regulated
ADORA3	0.0077	1.224925	up-regulated
BNIP3L	0.000774	0.870023	up-regulated
SDHB	0.000133	–0.61082	down-regulated
LY96	0.0168	0.737435	up-regulated
DPP9	0.00000154	0.628471	up-regulated
NLRP3	0.00619	0.805065	up-regulated
TAC1	0.00444	–1.39572	down-regulated
NEK7	0.0307	0.660205	up-regulated
GLMN	0.000404	–0.62616	down-regulated
CASP7	0.00545	0.615276	up-regulated
CASP1	0.0188	0.868561	up-regulated
HSP90AA1	5.49×10^{-6}	0.958937	up-regulated
AIM2	0.0315	0.74194	up-regulated
CHI3L1	0.0417	1.10387	up-regulated
CHMP6	0.000324	–0.64061	down-regulated
CEBPB	0.000582	0.707662	up-regulated
USF2	0.00111	0.666251	up-regulated

Note: *NLRP3*, nucleotide-binding oligomerization domain-like receptor protein 3; *HSP90AA1*, heat shock protein 90 kDa alpha family class A member 1; *VEGFA*, vascular endothelial growth factor-A; *CEBPB*, CCAAT/enhancer binding protein beta.

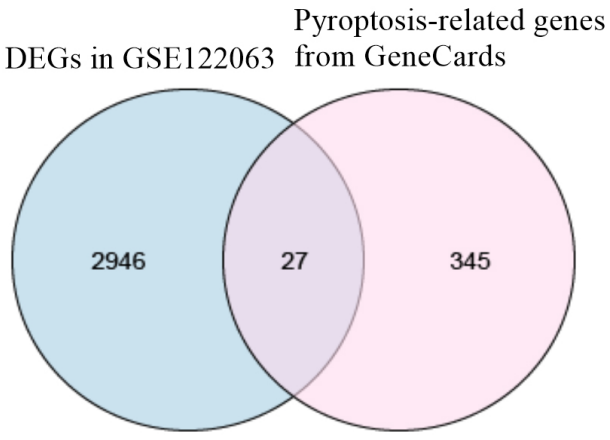

Fig. 3. Identification of pyroptosis-related DEGs in VaD. Venn diagram showing the intersection between total DEGs in GSE122063 and pyroptosis-related genes from GeneCards.

PPI Network Construction and Identification of Hub Pyro-DEGs

To further characterize the protein-protein interaction (PPI) of the 27 Pyro-DEGs, they were imported into the String database to construct a PPI network with the cut-off criterion of confidence score > 0.4. The obtained PPI network had 20 nodes and 76 edges, with 20 of 27 Pyro-DEGs identified as interacting with each other (Fig. 5). The PPI network was generated and displayed using Cytoscape software version v3.8.2. Seven genes (*GSDMB*, *BST2*, *PKN2*, *BNIP3L*, *SDHB*, *DPP9*, and *CHMP6*) that did not interact with any nodes in the PPI network were discarded in further analysis. The top nine genes (*NLRP3*, *TLR2*, *CASP*1, heat shock protein 90 kDa alpha family class A member 1 (*HSP90AA1*), vascular endothelial growth factor-A (*VEGFA*), *AIM2*, *LY96*, CCAAT/enhancer binding protein beta (*CEBPB*), and *BTK*) in the PPI network were regarded as hub Pyro-DEGs using Cytoscape software version v3.8.2 based on at least three types of algorithms (MCC, MNC, Degree) (Table 2).

Table 2. Node score of the top-ranked pyroptosis-related hub DEGs in the dataset GSE122063 based on the Maximal Clique Centrality (MCC), Maximum Neighborhood Component (MNC), and Degree algorithms of Cytoscape software version v3.8.2.

Gene.symbol	MCC	MNC	Degree
NLRP3	51	9	20
TLR2	51	9	20
CASP1	48	8	16
HSP90AA1	33	6	14
VEGFA	33	5	16
AIM2	12	4	8
LY96	8	4	8
CEBPB	7	3	8
BTK	7	3	8

Construction of TF-miRNA-Target Gene Interaction Network

First, nine hub Pyro-DEGs were introduced into the online miRNet v2.0 dataset to predict the upstream miRNAs that target them. There were a total of 431 miRNAs predicted to target these Pyro-DEGs. These miRNAs were then intersected with the differentially expressed miRNAs (DEMs) in the dataset GSE120584 to obtain 22 overlapping DEMs (Fig. 6A, Table 3). Based on the inclusion criteria of pairing inversed expression profiles of miRNAs and mRNAs, 15 of the 22 overlapping DEMs were identified to target five of the nine hub Pyro-DEGs. These 15 miRNAs were then used to build a miRNA-target gene network (Fig. 6B, Table 3). In this regulatory network, four unre-

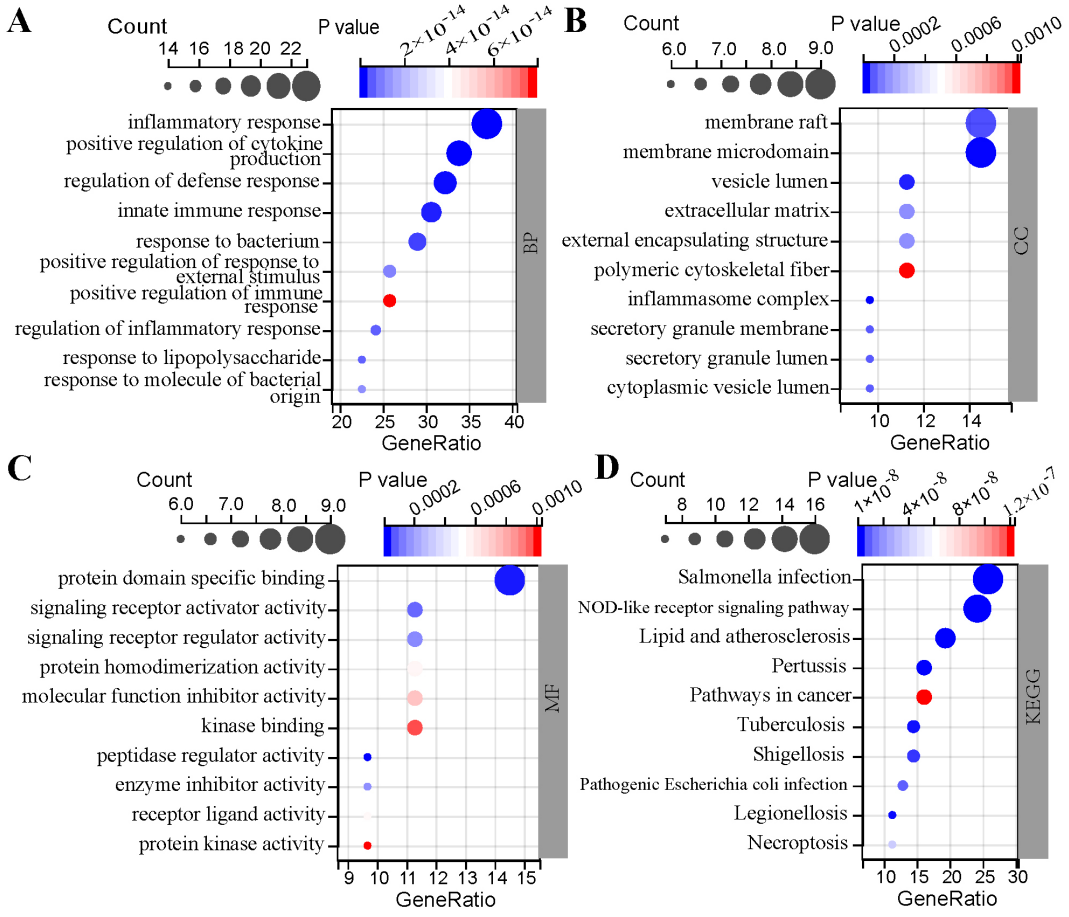

Fig. 4. GO enrichment and KEGG pathway analysis of 27 pyroptosis-related DEGs. (A) Ten top-ranked BP terms. (B) Ten top-ranked MF terms. (C) Ten top-ranked CC terms. (D) Ten top-ranked KEGG pathways. GO, gene ontology; BP, biological process; MF, molecular function; CC, cellular component; KEGG, Kyoto Encyclopedia of Genes and Genomes; DEGs, differentially expressed genes.

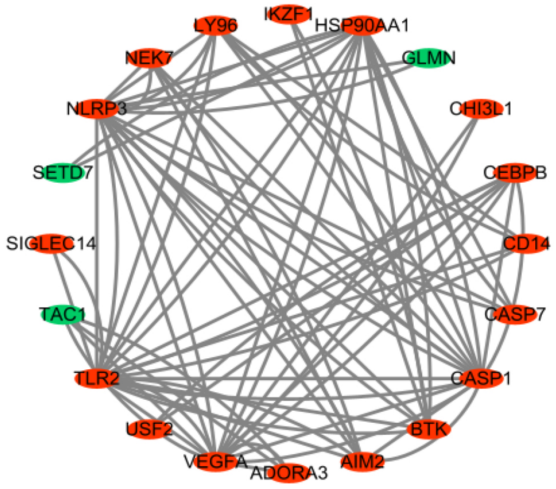

Fig. 5. PPI network of 27 pyroptosis-related DEGs. PPI network was visualized using Cytoscape software version v3.8.2. Green nodes represent down-regulated genes and red nodes represent up-regulated genes. DEGs, differentially expressed genes; PPI, protein-protein interaction.

lated miRNA-target gene pairs (*miR-4269-BTK*, *miR-92a-3p-BTK*, *miR-92a-3p-CASP1*, *miR-1236-3p-CASP1*) were eliminated from further analysis.

Next, 12 overlapping DEMs that target hub Pyro-DEGs (*VEGFA*, *HSP90AA1*, *CEBPB*) in the miRNA-target gene network were introduced into the TransmiR v2.0 dataset to predict the upstream TFs that interact with these DEMs. A total of 245 TFs were predicted and subsequently intersected with the total DEGs in GSE122063 to obtain 31 overlapping DE-TFs (Fig. 6C, **Supplementary Table 3**). These TF-miRNA pairs were then applied to create a TF-miRNA network and visualized using Cytoscape software version v3.8.2. The TF-miRNA network eventually contained 31 DE-TFs, 10 DEMs, and 100 interactions between the DE-TFs and their target DEMs (Fig. 6D).

Furthermore, the miRNA-target gene network and the TF-miRNA network were merged using the network merge operation of Cytoscape software version v3.8.2 to create a regulatory network among TFs, miRNAs, and target genes (Fig. 7). This regulatory network consists of 43 nodes, 116 edges, and two types of interactions: the TF-miRNA and miRNA-target gene actions.

Journal of
BIOLOGICAL REGULATORS
and Homeostatic Agents

Table 3. The 22 overlapping differentially expressed miRNAs (DEMs) in dataset GSE120584 and their target genes from GSE122063.

Gene.symbol	adj.*p*.Val	Log2(FC)	changes	Predicted target
miR-92a-3p	0.00000503	–0.98377	down-regulated	*BTK* (up), *CASP1* (up)
miR-6133	0.00000724	0.822513	up-regulated	none
miR-4269	0.00003	–0.82052	down-regulated	*BTK* (up)
miR-3646	0.00252	–0.77139	down-regulated	*VEGFA* (up)
miR-24-3p	0.00000653	–0.749	down-regulated	*HSP90AA1* (up), *VEGFA* (up)
miR-1304-3p	0.00308	–0.72479	down-regulated	*HSP90AA1* (up)
miR-1293	0.000269	–0.70059	down-regulated	*HSP90AA1* (up), *VEGFA* (up)
miR-125a-3p	0.000219	0.663917	up-regulated	none
miR-1236-3p	0.00000534	–0.64988	down-regulated	*CASP1* (up)
miR-191-5p	0.0021	–0.57594	down-regulated	*VEGFA* (up), *CEBPB* (up)
miR-23a-3p	0.000134	–0.57358	down-regulated	*HSP90AA1* (up)
miR-30d-5p	0.000615	–0.56737	down-regulated	*HSP90AA1* (up), *VEGFA* (up)
miR-3184-5p	0.0000322	0.562125	up-regulated	none
miR-320a	0.00000396	0.553367	up-regulated	none
miR-4732-5p	0.00458	–0.55016	down-regulated	*HSP90AA1* (up)
miR-4792	0.0000925	–0.54822	down-regulated	*VEGFA* (up)
miR-5193	0.0000315	–0.53926	down-regulated	*VEGFA* (up)
miR-522-5p	0.000623	0.537903	up-regulated	none
miR-642b-5p	0.0267	–0.52075	down-regulated	*VEGFA* (up)
miR-670-5p	0.000254	–0.513	down-regulated	*VEGFA* (up)
miR-6754-3p	0.0000017	0.512345	up-regulated	none
miR-6859-5p	0.000252	0.50305	up-regulated	none

Finally, the NetworkAnalyzer plug-in in Cytoscape software version v3.8.2 was applied to analyze the topological properties of the TF-miRNA-target gene interaction network. The top-ranked three key target genes, five miRNAs, and five TFs with high degrees are presented in Table 4.

Receiver Operating Characteristic (ROC) Curve Analysis

Based on the expression data in GSE122063 and GSE120584, ROC analysis was carried out on the top-ranked nodes in our TF-miRNA-target gene regulatory network, which included two key target genes (*VEGFA* and *HSP90AA1*), five key miRNAs (*miR-1304-3p*, *miR-191-5p*, *miR-23a-3p*, *miR-1293*, *miR-5193*), and five key TFs (Early Growth Response Protein 1 (*EGR1*), runt-related transcription factor-1 (*RUNX1*), *SPI1*, PHD finger protein 8 (*PHF8*), *CEBPB*). AUC values were calculated for each key component. The AUC of key target genes and key TFs were all greater than 0.7, including *VEGFA* ($p < 0.05$), *HSP90AA1* ($p < 0.05$), *EGR1* ($p < 0.05$), *RUNX1* ($p < 0.05$), *SPI1* ($p < 0.05$), *PHF8* ($p < 0.05$), *CEBPB* ($p < 0.05$) (Fig. 8A–G). The AUC of key miRNAs was calculated, including *miR-1304-3p* (AUC = 0.700, $p < 0.05$), *miR-1293* (AUC = 0.689, $p < 0.05$), *miR-191-5*p (AUC = 0.582, $p < 0.05$), *miR-23a-3p* (AUC = 0.554, $p > 0.05$), *miR-5193* (AUC = 0.689, $p < 0.05$) (Fig. 8H–L). Except for *miR-23a-3p*, other key components were identified as potential biomarkers of VaD. The *p*-value for *miR-23a-3p* failed to reach statistical significance, so *miR-23a-3p* could not be regarded as a potential biomarker for VaD.

Verification of Key Nodes in SH-SY5Y Cell Injury Induced by Oxygen-Glucose Deprivation (OGD)

To validate the key nodes in the regulatory network, RT-qPCR was used to analyze the expression levels of the key target genes, miRNAs, and TFs in OGD-triggered SH-SY5Y cell injury. OGD-induced SH-SY5Y cell injury is widely used as an *in vitro* model to study cerebral ischemic stroke [15]. The RT-qPCR analysis of the genes in OGD-stimulated SH-SY5Y cell injury revealed that the mRNA expressions of two key target genes (*VEGFA* and *HSP90AA1*) and five key TFs (*CEBPB*, *RUNX1*, *SPI1*, and *PHF8*) were significantly up-regulated, while the transcript expressions of key TF *EGR1* and five key miRNAs (*miR-1304-3p*, *miR-191-5p*, *miR-23a-3p*, *miR-1293*, *miR-5193*) were markedly down-regulated in the OGD group than those in the control group (Fig. 9A–L. $p < 0.01$ for *VEGFA*, *HSP90AA1*, *SPI1*, *EGR1*, *miR-1293*, *miR-191-5p*, and *miR-5193*; $p < 0.05$ for *CEBPB*, *RUNX1*, *PHF8*, *miR-1304-3p*, and *miR-23a-3p*). The changing trend of most predicted key nodes in our OGD-stimulated SH-SY5Y cell injury was similar to that in the microarray analysis in GSE122063 and GSE120584. The results revealed that the relationships between the hub target genes and the corresponding miRNAs or between the target miRNAs and their corresponding TFs in the TF-miRNA-target gene network were reliable.

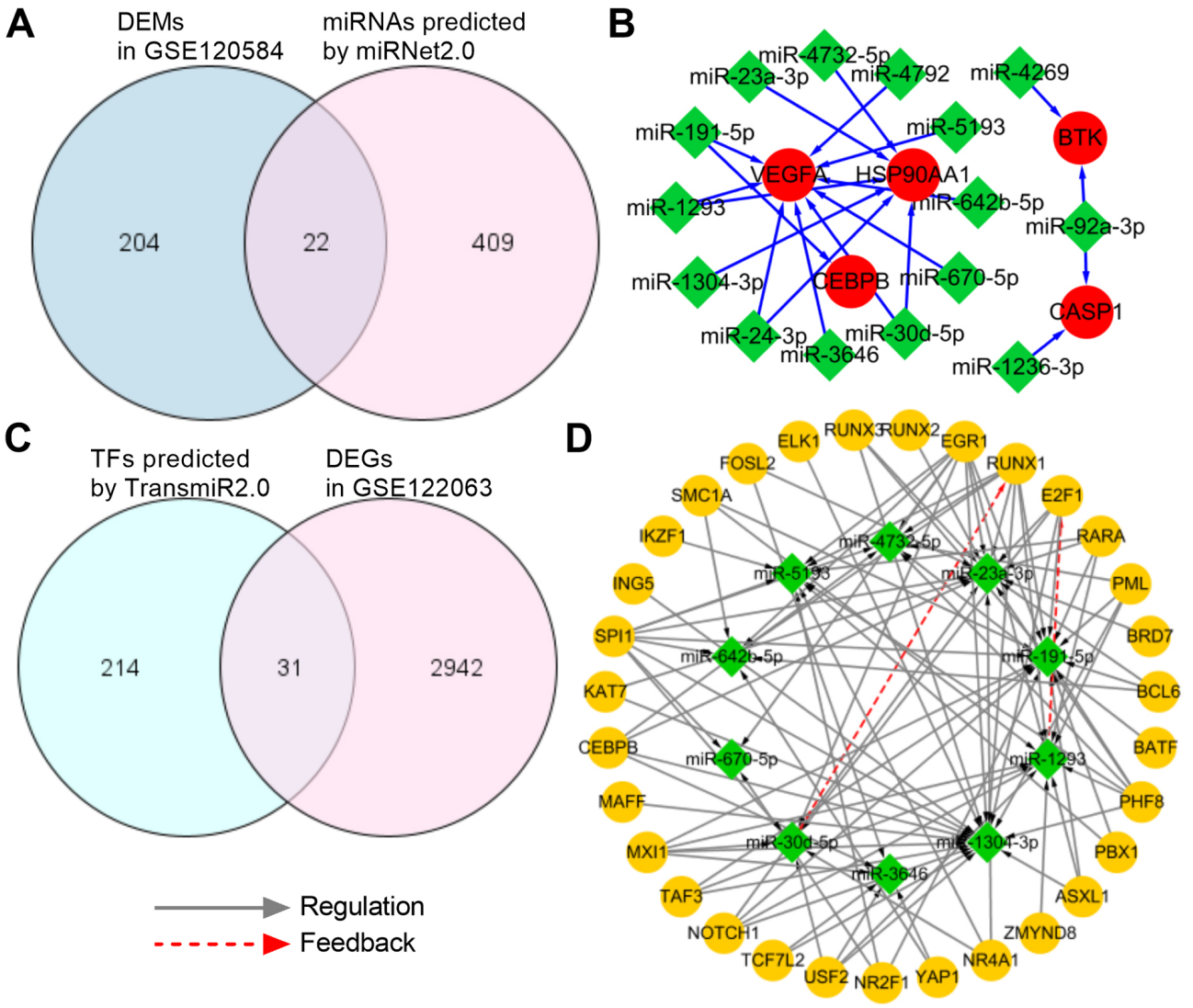

Fig. 6. Construction of miRNA-target gene and TF-miRNA interaction networks. (A) Venn diagram revealing the intersection between total DEMs in GSE120584 and the predicted miRNAs by miRNet v2.0. (B) miRNA-target gene network. (C) Venn diagram demonstrating the intersection between total DEGs in GSE122063 and the predicted TFs by TransmiR v2.0. (D) TF-miRNA network. Red nodes indicate the target genes that were targeted by miRNAs, green nodes represent the miRNAs, and orange nodes represent the TFs. DEGs, differentially expressed genes; TFs, transcription factors; miRNAs, microRNAs; DEMs, differentially expressed miRNAs.

Drug-Gene Interaction Analysis

To explore the treatment for VaD, the DGIdb database was used to predict potential drugs that target biomarkers. The analysis identified 210 drugs or compounds targeting 4 marker genes (*VEGFA*, *HSP90AA1*, *EGR1*, and *RUNX1*), as shown in **Supplementary Table 4**. Most drug-gene interaction types were unknown, except for 16 known types that were all inhibitory for *VEGFA* and *HSP90AA1* (Fig. 10). Among the 16 drugs that exert inhibitory effects on *VEGFA* and *HSP90AA1*, nine drugs belong to the antineoplastic agents, and two drugs (ranibizumab and pegaptanib sodium) are used for the treatment of age-related macular degeneration.

Discussion

Dementia is a significant global challenge for health and social care in the 21st century. Age is one of the most substantiated risk factors for ischemia brain injury, and as a result, the number of individuals affected by VaD is predicted to increase over time [16,17]. However, it is challenging to understand the pathogenesis of VaD and identify novel therapeutic strategies to effectively alleviate VaD symptoms.

The role of inflammation-associated pyroptosis in VaD has not been extensively studied. In this study, key genes related to pyroptosis and VaD were identified using bioinformatic analysis. A total of 27 pyroptosis-related genes were found to be differentially expressed in the brain

Journal of
BIOLOGICAL REGULATORS
and Homeostatic Agents

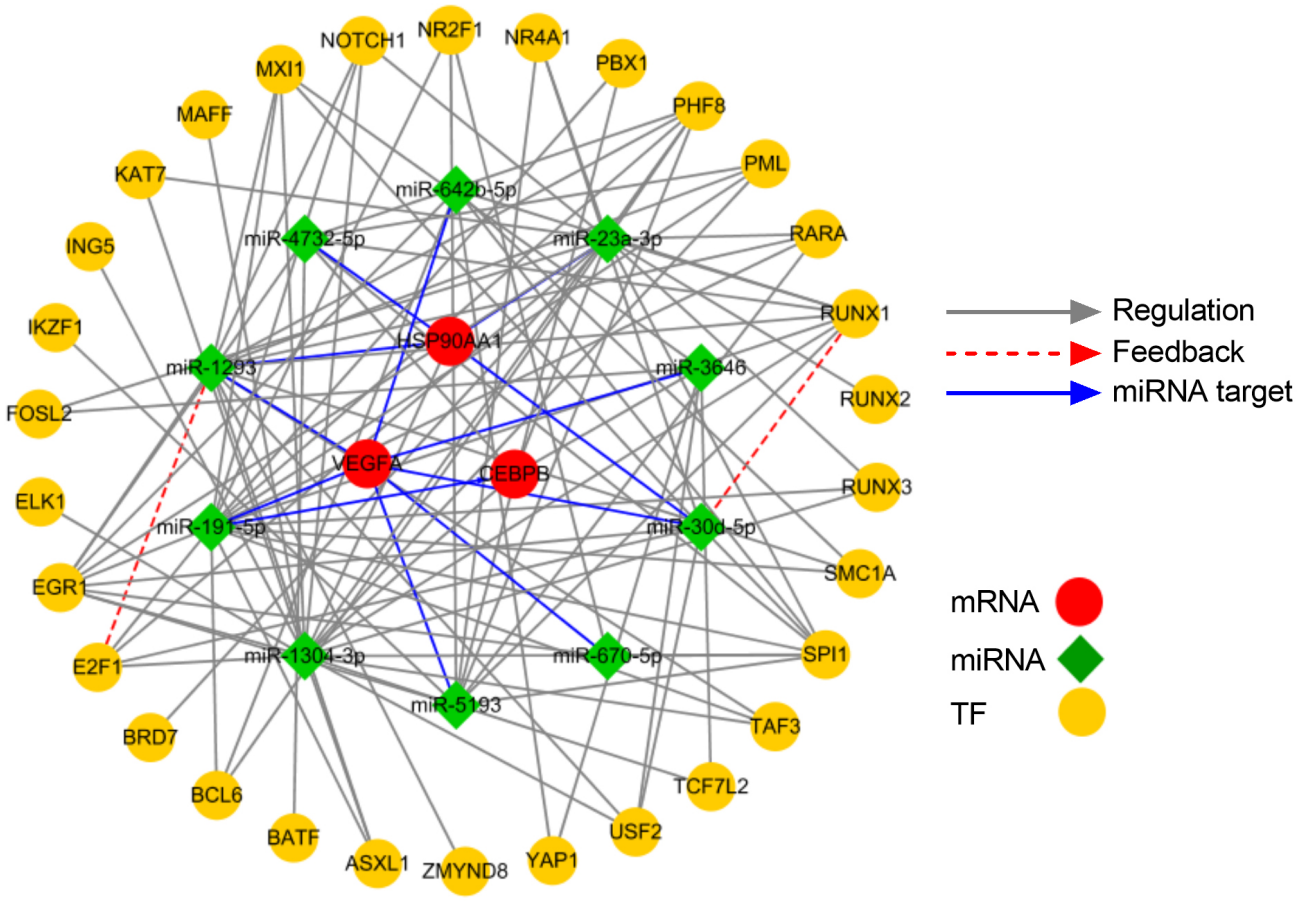

Fig. 7. Construction of the TF-miRNA-target gene interaction network. TF-miRNA-target gene interaction network was established using Cytoscape software version v3.8.2. Red nodes indicate the target genes that were targeted by miRNAs, green nodes represent the miRNAs, and orange nodes represent the TFs. TFs, transcription factors; miRNAs, microRNAs.

Table 4. Topological score of the top-ranked nodes in the transcription factor-microRNA (TF-miRNA)-target gene interaction network.

Gene symbol	Attribution	Average shortest path length	Betweenness centrality	Closeness centrality	Degree
miR-1304-3p	miRNA	1.880952	0.265651	0.531646	19
miR-191-5p	miRNA	1.928571	0.175533	0.518519	18
miR-23a-3p	miRNA	2.02381	0.2037	0.494118	16
miR-1293	miRNA	2.071429	0.127894	0.482759	15
miR-5193	miRNA	2.309524	0.089041	0.43299	10
Early Growth Response Protein 1 (*EGR1*)	TF	1.809524	0.080633	0.552632	9
Runt-related transcription factor-1 (*RUNX1*)	TF	1.857143	0.06213	0.538462	8
SPI1	TF	1.904762	0.064684	0.525	8
PHD finger protein 8 (*PHF8*)	TF	2	0.037673	0.5	6
CEBPB	TF/Target gene	2.095238	0.031742	0.477273	5
VEGFA	Target gene	2.238095	0.04223	0.446809	7
HSP90AA1	Target gene	2.190476	0.020707	0.456522	5

samples from VaD patients, nine of which were identified as pyroptosis-related hub genes. GO enrichment analyses revealed that these pyroptosis-related DEGs were mainly enriched in the inflammatory response, positive regulation of response to external stimulus, positive regulation of cytokine production, regulation of defense response, etc. KEGG pathway enrichment analysis revealed that these pyroptosis-related DEGs were enriched in salmonella infection, NOD-like receptor signaling pathway, and lipid and atherosclerosis. It is worth noting that under endogenous and/or exogenous stimuli, activation of the NOD-like receptor signaling pathway is essential for the initiation of

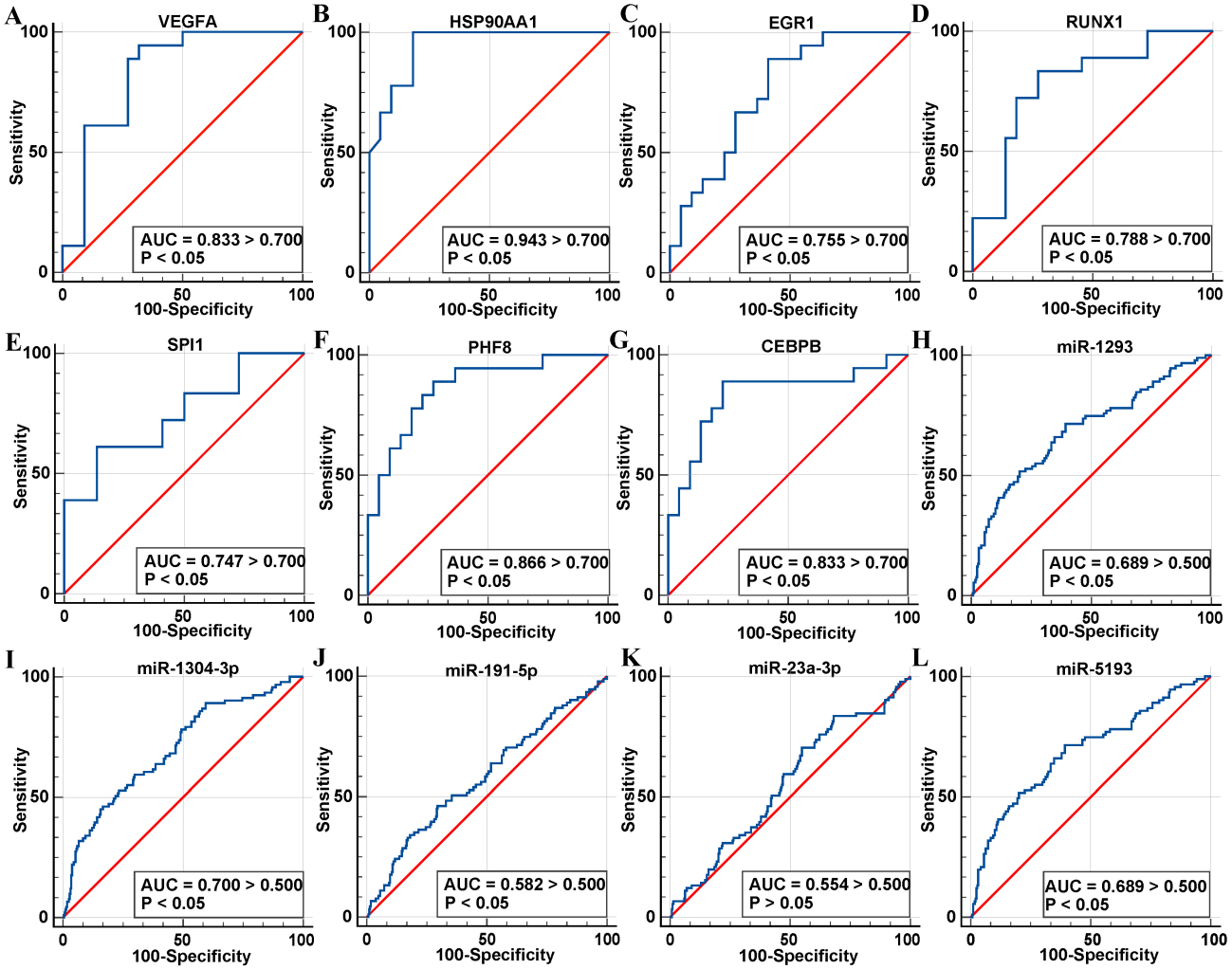

Fig. 8. Receiver operating characteristic (ROC) curve of the top-ranked nodes in our TF-miRNA-target gene interaction network. (A) ROC for *VEGFA*. (B) ROC for *HSP90AA1*. (C) ROC for *EGR1*. (D) ROC for *RUNX1*. (E) ROC for *SPI1*. (F) ROC for *PHF8*. (G) ROC for *CEBPB*. (H) ROC for *miR-1293*. (I) ROC for *miR-1304-3p*. (J) ROC for *miR-191-5p*. (K) ROC for *miR-23a-3p*. (L) ROC for *miR-5193*. Key target genes and key TFs with AUC larger than 0.7 and *p* less than 0.05 were regarded as potential biomarkers. Key miRNAs with AUC larger than 0.5 and *p* less than 0.05 were identified as potential biomarkers. AUC, area under the curve.

pyroptosis [18]. The activated NOD-like receptor signaling pathway initiates pyroptosis by promoting the secretion of pro-inflammatory factors IL-1β and IL-18 and the activation of Gasdermin-D. Pyroptosis has been shown to aggravate traumatic brain injury [19]. Conversely, suppression of NLRP3 inflammasome reportedly improves diabetes-mediated blood-brain barrier (BBB) damage and cognitive impairment in rats [7]. Additionally, the NOD-like receptor signaling pathway mediates cell death and neuronal loss during the progression of vascular cognitive impairment [20]. Thus, these identified pyroptosis-related hub genes may play a key role in mediating VaD and serve as potential therapeutic targets for VaD.

In this study, the vascular endothelial growth factor-A (*VEGFA*) and the heat shock protein 90 kDa alpha family class A member 1 (*HSP90AA1*) were identified as pyroptosis-related hub genes in our TF-miRNA-target gene interaction network, and further as VaD-associated biomarkers. These two genes have been identified in previous studies on inflammatory diseases [21,22]. Astrocyte-derived *VEGFA* is believed to be a key driver of BBB disruption in inflammatory central system disease [23]. Down-regulation of astrocyte-derived *VEGFA* contributes to the improvement of experimental stroke by repairing the BBB [24]. *HSP90AA1* belongs to one of the stress-inducible mammalian cytosolic heat shock protein 90-alpha (HSP90α) family. HSP90α acts as key chaperones to regulate the biological activity of various protein substrates, among which there are some key signaling molecules (e.g., nuclear factor-kappa B) that are involved in inflammation [25]. Besides their anti-tumor effects, HSP90 inhibitors have been demonstrated to attenuate inflammation [26]. *HSP90AA1* has been shown to have pro-inflammatory effects in lipopolysaccharide-stimulated human gingival fi-

Journal of
BIOLOGICAL REGULATORS
and Homeostatic Agents

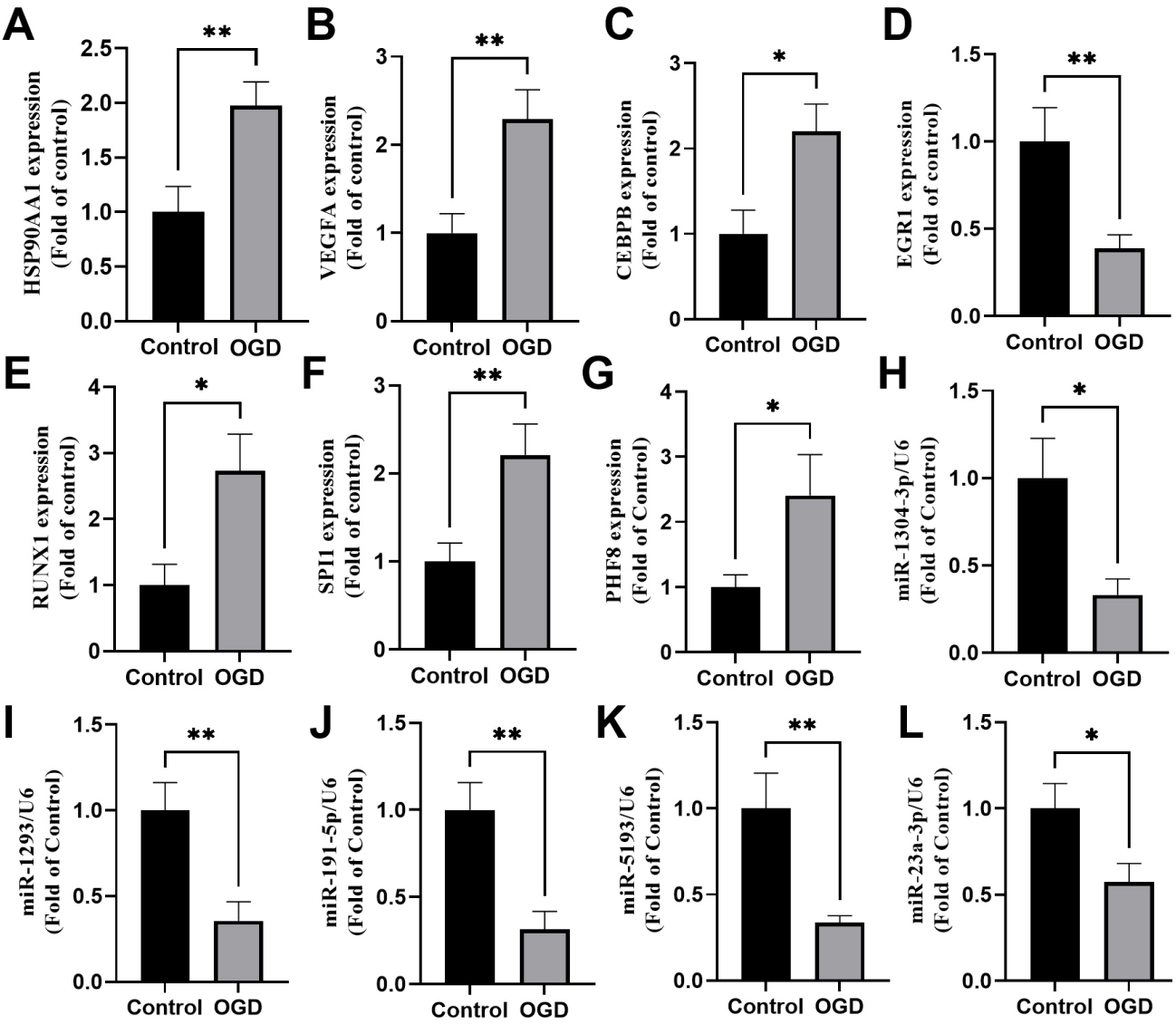

Fig. 9. Verification of the key nodes in the regulatory network using oxygen-glucose deprivation (OGD)-stimulated SH-SY5Y cell model. SH-SY5Y cells were cultured in oxygen-glucose-free Dulbecco's Modified Eagle's Medium (DMEM) for 24 h to produce lethal OGD. Immediately after applying OGD, cells were harvested for real-time quantitative polymerase chain reaction (RT-qPCR) analysis of mRNA or miRNA expression of key nodes including key target genes *HSP90AA1* and *VEGFA* mRNA (A,B), key TFs (*CEBPB*, *EGR1*, *RUNX1*, *SPI1*, and *PHF8*) (C–G), and key miRNAs (*miR-1304-3p*, *miR-1293*, *miR-191-5p*, *miR-5193*, and *miR-23a-3p*) (H–L). $^{*}p < 0.05$, $^{**}p < 0.01$ *vs* Control.

broblasts [22]. Suppression of *HSP90AA1* has been reported to inhibit the apoptosis of human gingival fibroblasts [22]. Therefore, modulation of *VEGFA* and *HSP90AA1* may regulate inflammation and pyroptosis in VaD.

Ten down-regulated miRNAs were identified as key genes, and four of these miRNAs were identified as VaD-associated biomarkers, including *miR-1304-3p*, *miR-1293*, *miR-191-5p*, and *miR-5193*. The *miR-191-5p* has been reported to suppress NLRP3 inflammasome activation in retinal pigment epithelium cell injury induced by amyloid-β1-40 [27] and attenuate sepsis-triggered acute kidney injury in rats [28]. *miR-191-5p* down-regulation was found in mice and patients with Alzheimer's disease [29,30]. Conversely, *miR-191-5p* overexpression attenuated microglial cell injury and neuronal cell death in Alzheimer's disease [30]. However, other miRNAs have been rarely studied, and the results of this study are required to be validated in further studies.

In this study, 31 differentially expressed TFs were identified as miRNA-associated key genes, among which five TFs were identified as VaD-related biomarkers. These five TFs are *EGR1*, *RUNX1*, *SPI1*, *PHF8*, and *CEBPB*. Early Growth Response Protein 1 (*EGR1*), which is the only down-regulated key TF identified as a VaD-related biomarker, has been involved in cerebral inflammation and ischemic stroke [31,32]. However, some results from dif-

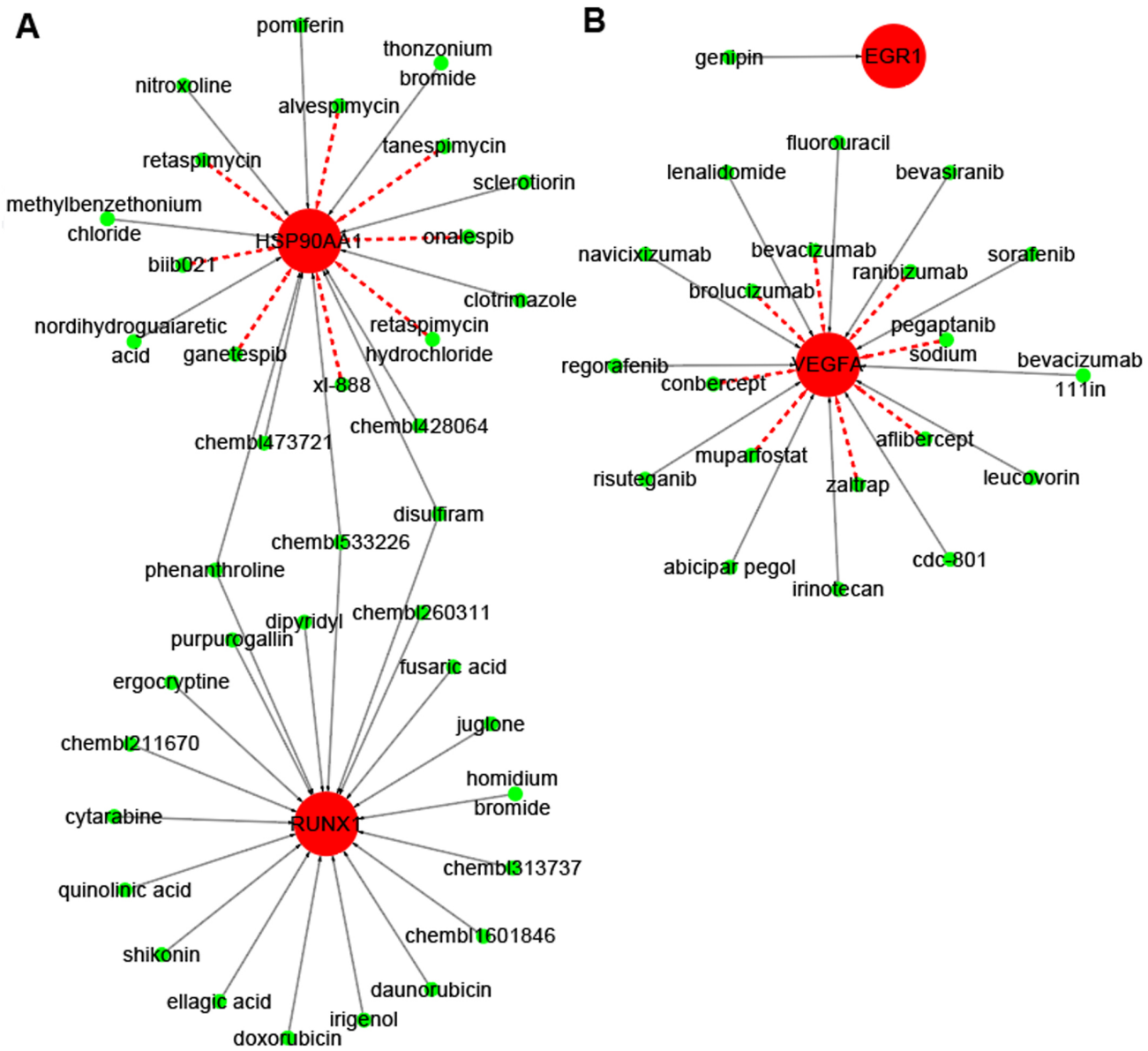

Fig. 10. Drug-target gene interaction analysis. (A) Representative drug-target gene interactions for *HSP90AA1* and *RUNX1*. (B) Representative drug-target gene interactions for *EGR1* and *VEGFA*. Red nodes indicated target genes. Green nodes indicated predicted drugs. Red lines indicated the inhibitory effects of predicted drugs on target genes. Grey lines indicated unknown effects of predicted drugs on target genes.

ferent groups were contradictory. Some studies revealed that *EGR1* activation promoted inflammation and ischemic brain damage [33–35], while *EGR1* knockout inhibited them. Conversely, Ducruet *et al.* [36] found that *EGR1* knockout exacerbated ischemic brain damage despite a reduction in inflammation. Zhu *et al.* [37] suggested that stably expressed *EGR1* might contribute to keeping the brain cholinergic signaling intact in early Alzheimer's disease stages, whilst down-regulated *EGR1* might induce the neurodegeneration of the cholinergic nucleus during late stages. Therefore, *EGR1* is believed to have a versatile role in VaD. Runt-related transcription factor-1 (*RUNX1*) is a key mediator of neuronal differentiation [38] that mediates lipopolysaccharide-induced lung inflammation through interaction with the nuclear factor-kappa B (NF-κB) pathway [39]. Conversely, inhibition of *RUNX1* attenuates hepatic inflammation and immune cell infiltration in the murine models of non-alcoholic steatohepatitis [40]. *RUNX1* expression is induced in activated microglial cells and GFAP-expressing neural stem cells from neurogenic regions in mice with traumatic brain injury [41], suggesting the role of *RUNX1* in mediating neuroinflammation. The spleen focus forming virus (SFFV) proviral integration oncogene spi1 (*SPI1*), also known as PU.1, is up-regulated in rats with spinal cord injury (SCI) and contributes to microglial-mediated inflammation through interaction with the NF-κB

Journal of
BIOLOGICAL REGULATORS
and Homeostatic Agents

p50 subunit [42]. Meanwhile, reduced PU.1 expression is protective, while high *SPI1* expression is linked to higher risk for Alzheimer's disease (AD) [43,44]. Proteomic analysis has revealed that PHD finger protein 8 (*PHF8*) plays a key role in Toll-like receptor 4 (TLR4)-mediated acute inflammation in lipopolysaccharide-stimulated macrophages [45]. Furthermore, *PHF8* knockout mice showed a deficit in learning and memory, suggesting a potential role of *PHF8* in mediating mental retardation [46]. As key regulatory TF, CCAAT/enhancer binding protein beta (*CEBPB*) is up-regulated in AD [47] and has been shown to activate the downstream δ-secretase, promoting the production of neurotoxic amyloid β protein and tau protein [48]. Although the prognostic value of these TFs in VaD has been seldom reported in previous studies [49,50], the functional implication of these TFs should not be ignored. In the present study, ROC analysis identified these TFs as key biomarkers for VaD. These dysregulated TFs were found to be associated with miRNAs in VaD for the first time. Further studies are required to validate the potential roles of these TFs in regulating miRNAs related to VaD.

Currently, cholinesterase inhibitors and excitatory amino acid receptor antagonists are the primary preventive medications used for the treatment of VaD [51,52]. These drugs show anti-inflammatory effects and can improve the symptoms of VaD [53,54]. In this study, four biomarker genes (*VEGFA*, *HSP90AA1*, *EGR1*, and *RUNX1*) were identified as important target genes for drug screening. This study identified 210 drugs targeting four marker genes (*VEGFA*, *HSP90AA1*, *EGR1*, and *RUNX1*), 16 of which were inhibitory for *VEGFA* and *HSP90AA1*. Among the screened drugs, the HSP90 inhibitor Tanespimycin, also known as 17-AAG, was demonstrated to attenuate amyloid-β-induced synaptic toxicity and memory deficit in a Tg2576 mouse model with Alzheimer's disease [55]. Tanespimycin has been found to ameliorate transient global cerebral ischemia-induced memory deficit and hippocampal CA1 neuronal autophagic death [56]. Bevacizumab, an anti-VEGF antibody, has been reported to improve cognition and blood-brain barrier leakage in patients with radiation-induced brain necrosis [57,58]. Aflibercept, a vascular endothelial growth factor-A (VEGFA)-trap, has been found to reduce stroke-induced vascular permeability and brain swelling in obese mice [59]. Therefore, the efficacy of these three drugs in VaD treatment should be evaluated in future studies.

Conclusions

We identified 27 pyroptosis-related differentially expressed genes (Pyro-DEGs) in GSE122063, 24 overlapping differentially expressed miRNAs (DEMs) in GSE120584, and 31 overlapping DE-TFs in GSE122063. A VaD-related TF-miRNA-target gene interaction network was created, which contained 31 TFs, 10 miRNAs, and 3 target genes. Among these key components in the network, two key target genes (*VEGFA* and *HSP90AA1*), four miRNAs (*miR-1304-3p*, *miR-1293*, *miR-191-5p*, and *miR-5193*), and five TFs (*EGR1*, *RUNX1*, *SPI1*, *PHF8*, and *CEBPB*) were identified as VaD-related biomarkers. Drug-target gene interaction analysis identified three potential drugs targeting *HSP90AA1* and *VEGFA* for the treatment of VaD. The identified pyroptosis-related hub genes, key DEMs, and DE-TFs in our regulatory network were associated with VaD. Therefore, our findings suggest that the TF-miRNA-target gene interaction network may be involved in VaD, and *HSP90AA1* and *VEGFA* can be the core genes associated with VaD and represent potential therapeutic targets for VaD treatment.

Abbreviations

VaD, vascular dementia; TF, transcription factor; miRNA, microRNA; PPI, protein-protein interaction; DEGs, differentially expressed genes; NLRP3, nucleotide-binding oligomerization domain-like receptor protein 3; GO, gene ontology; Pyro-DEG, pyroptosis-related differentially expressed gene; KEGG, Kyoto Encyclopedia of Genes and Genomes; DEMs, differentially expressed miRNAs; DE-TFs, differentially expressed transcription factors; ROC, receiver operating characteristic.

Availability of Data and Materials

The datasets analyzed during the current study are available in the GEO database (https://www.ncbi.nlm.nih.gov/geo/). The accession numbers of GEO datasets are GSE122063 and GSE120584. All data are available from the corresponding author upon reasonable request.

Author Contributions

QY, HY, and BM designed the study. QY, HY, SW, and BM performed the research. QY, HY, and SW collected and analyzed the data. QY and BM contributed to the writing of the manuscript. All authors contributed to editorial changes in the manuscript. All authors read and approved the final manuscript. All authors agreed to be accountable for all aspects of the work in ensuring that questions related to the accuracy or integrity of any part of the work are appropriately investigated and resolved.

Ethics Approval and Consent to Participate

Not applicable.

Acknowledgment

Not applicable.

Funding

This research was funded by the Chengdu Medical Research Project (Grant# 2022151).

Conflict of Interest

The authors declare no conflict of interest.

Supplementary Material

Supplementary material associated with this article can be found, in the online version, at https://doi.org/10.23812/j.biol.regul.homeost.agents.20243805.293.

References

[1] Wolters FJ, Ikram MA. Epidemiology of Vascular Dementia. Arteriosclerosis, Thrombosis, and Vascular Biology. 2019; 39: 1542–1549.

[2] O'Brien JT, Thomas A. Vascular dementia. Lancet (London, England). 2015; 386: 1698–1706.

[3] Iadecola C, Duering M, Hachinski V, Joutel A, Pendlebury ST, Schneider JA, *et al*. Vascular Cognitive Impairment and Dementia: JACC Scientific Expert Panel. Journal of the American College of Cardiology. 2019; 73: 3326–3344.

[4] Ohto U. Activation and regulation mechanisms of NOD-like receptors based on structural biology. Frontiers in Immunology. 2022; 13: 953530.

[5] Li Q, Shen L, Liang P, Dong Y, Fang T, Wang L, *et al*. Dl-3-n-Butylphthalide Protects against Memory Deficits in Vascular Dementia Rats by Attenuating Pyroptosis via TLR-4/NF-κB Signaling Pathway. Neuropsychobiology. 2023; 82: 150–157.

[6] Liu L, Wang N, Kalionis B, Xia S, He Q. HMGB1 plays an important role in pyroptosis induced blood brain barrier breakdown in diabetes-associated cognitive decline. Journal of Neuroimmunology. 2022; 362: 577763.

[7] Ward R, Li W, Abdul Y, Jackson L, Dong G, Jamil S, *et al*. NLRP3 inflammasome inhibition with MCC950 improves diabetes-mediated cognitive impairment and vasoneuronal remodeling after ischemia. Pharmacological Research. 2019; 142: 237–250.

[8] Han X, Zhou L, Tu Y, Wei J, Zhang J, Jiang G, *et al*. Circulating exo-miR-154-5p regulates vascular dementia through endothelial progenitor cell-mediated angiogenesis. Frontiers in Cellular Neuroscience. 2022; 16: 881175.

[9] Ma X, Wang Y, Shi Y, Li S, Liu J, Li X, *et al*. Exosomal miR-132-3p from mesenchymal stromal cells improves synaptic dysfunction and cognitive decline in vascular dementia. Stem Cell Research & Therapy. 2022; 13: 315.

[10] Zhai W, Zhao M, Zhang G, Wang Z, Wei C, Sun L. MicroRNA-Based Diagnosis and Therapeutics for Vascular Cognitive Impairment and Dementia. Frontiers in Neurology. 2022; 13: 895316.

[11] Chen C, Chen H, Zhang Y, Thomas HR, Frank MH, He Y, *et al*. TBtools: An Integrative Toolkit Developed for Interactive Analyses of Big Biological Data. Molecular Plant. 2020; 13: 1194–1202.

[12] Shen W, Song Z, Zhong X, Huang M, Shen D, Gao P, *et al*. Sangerbox: A comprehensive, interaction-friendly clinical bioinformatics analysis platform. iMeta. 2022; 1: e36.

[13] Tong Z, Cui Q, Wang J, Zhou Y. TransmiR v2.0: an updated transcription factor-microRNA regulation database. Nucleic Acids Research. 2019; 47: D253–D258.

[14] Wang HF, Wang ZQ, Ding Y, Piao MH, Feng CS, Chi GF, *et al*. Endoplasmic reticulum stress regulates oxygen-glucose deprivation-induced parthanatos in human SH-SY5Y cells via improvement of intracellular ROS. CNS Neuroscience & Therapeutics. 2018; 24: 29–38.

[15] Zieliński T, Pabijan J, Zapotoczny B, Zemła J, Wesołowska J, Pera J, *et al*. Changes in nanomechanical properties of single neuroblastoma cells as a model for oxygen and glucose deprivation (OGD). Scientific Reports. 2022; 12: 16276.

[16] Finger CE, Moreno-Gonzalez I, Gutierrez A, Moruno-Manchon JF, McCullough LD. Age-related immune alterations and cerebrovascular inflammation. Molecular Psychiatry. 2022; 27: 803–818.

[17] Mahinrad S, Sorond F, Gorelick PB. The Role of Vascular Risk Factors in Cognitive Impairment and Dementia and Prospects for Prevention. Clinics in Geriatric Medicine. 2023; 39: 123–134.

[18] Kinra M, Nampoothiri M, Arora D, Mudgal J. Reviewing the importance of TLR-NLRP3-pyroptosis pathway and mechanism of experimental NLRP3 inflammasome inhibitors. Scandinavian Journal of Immunology. 2022; 95: e13124.

[19] Ge X, Li W, Huang S, Yin Z, Xu X, Chen F, *et al*. The pathological role of NLRs and AIM2 inflammasome-mediated pyroptosis in damaged blood-brain barrier after traumatic brain injury. Brain Research. 2018; 1697: 10–20.

[20] Poh L, Sim WL, Jo DG, Dinh QN, Drummond GR, Sobey CG, *et al*. The role of inflammasomes in vascular cognitive impairment. Molecular Neurodegeneration. 2022; 17: 4.

[21] Shibuya M. VEGF-VEGFR System as a Target for Suppressing Inflammation and other Diseases. Endocrine, Metabolic & Immune Disorders Drug Targets. 2015; 15: 135–144.

[22] Zhang H, Huang J, Fan X, Miao R, Wang Y. HSP90AA1 promotes the inflammation in human gingival fibroblasts induced by Porphyromonas gingivalis lipopolysaccharide via regulating of autophagy. BMC Oral Health. 2022; 22: 366.

[23] Argaw AT, Asp L, Zhang J, Navrazhina K, Pham T, Mariani JN, *et al*. Astrocyte-derived VEGF-A drives blood-brain barrier disruption in CNS inflammatory disease. The Journal of Clinical Investigation. 2012; 122: 2454–2468.

[24] Tan S, Shan Y, Lin Y, Liao S, Zhang B, Zeng Q, *et al*. Neutralization of interleukin-9 ameliorates experimental stroke by repairing the blood-brain barrier via down-regulation of astrocyte-derived vascular endothelial growth factor-A. FASEB Journal: Official Publication of the Federation of American Societies for Experimental Biology. 2019; 33: 4376–4387.

[25] Tukaj S, Sitko K. Heat Shock Protein 90 (Hsp90) and Hsp70 as Potential Therapeutic Targets in Autoimmune Skin Diseases. Biomolecules. 2022; 12: 1153.

[26] Costa TEMM, Raghavendra NM, Penido C. Natural heat shock protein 90 inhibitors in cancer and inflammation. European Journal of Medicinal Chemistry. 2020; 189: 112063.

[27] Chen J, Sun J, Hu Y, Wan X, Wang Y, Gao M, *et al*. MicroRNA-191-5p ameliorates amyloid-β_{1-40} -mediated retinal pigment epithelium cell injury by suppressing the NLRP3 inflammasome pathway. FASEB Journal: Official Publication of the Federation of American Societies for Experimental Biology. 2021; 35: e21184.

[28] Qin Y, Wang G, Peng Z. MicroRNA-191-5p diminished sepsis-induced acute kidney injury through targeting oxidative stress responsive 1 in rat models. Bioscience Reports. 2019; 39: BSR20190548.

[29] Wan W, Liu G, Li X, Liu Y, Wang Y, Pan H, *et al*. MiR-191-5p alleviates microglial cell injury by targeting Map3k12 (mitogen-activated protein kinase kinase kinase 12) to inhibit the MAPK (mitogen-activated protein kinase) signaling pathway in Alzheimer's disease. Bioengineered. 2021; 12: 12678–12690.

[30] Wang L, Shui X, Zhang M, Mei Y, Xia Y, Lan G, *et al*. MiR-191-5p Attenuates Tau Phosphorylation, Aβ Generation, and Neuronal Cell Death by Regulating Death-Associated Protein Kinase 1. ACS Chemical Neuroscience. 2022; 13: 3554–3566.

[31] Ko SW, Vadakkan KI, Ao H, Gallitano-Mendel A, Wei F, Milbrandt J, *et al*. Selective contribution of Egr1 (zif/268) to persistent inflammatory pain. The Journal of Pain. 2005; 6: 12–20.

[32] Li YY, Guo JH, Liu YQ, Dong JH, Zhu CH. PPARγ Activation-Mediated Egr-1 Inhibition Benefits Against Brain Injury in an Experimental Ischaemic Stroke Model. Journal of Stroke and Cerebrovascular Diseases: the Official Journal of National Stroke Association. 2020; 29: 105255.

[33] Tureyen K, Brooks N, Bowen K, Svaren J, Vemuganti R. Transcription factor early growth response-1 induction mediates inflammatory gene expression and brain damage following transient focal ischemia. Journal of Neurochemistry. 2008; 105: 1313–1324.

[34] Yu Q, Huang Q, Du X, Xu S, Li M, Ma S. Early activation of Egr-1 promotes neuroinflammation and dopaminergic neurodegeneration in an experimental model of Parkinson's disease. Experimental Neurology. 2018; 302: 145–154.

[35] Xie L, Wang Y, Chen Z. Early Growth Response Protein 1 Knockdown Alleviates the Cerebral Injury in Rats with Intracerebral Hemorrhage via STAT3/NF-κB Pathway by Reducing RXRα Acetylation Level. Neuroscience. 2022; 487: 120–130.

[36] Ducruet AF, Sosunov SA, Visovatti SH, Petrovic-Djergovic D, Mack WJ, Connolly ES, Jr, *et al*. Paradoxical exacerbation of neuronal injury in reperfused stroke despite improved blood flow and reduced inflammation in early growth response-1 gene-deleted mice. Neurological Research. 2011; 33: 717–725.

[37] Zhu QB, Unmehopa U, Bossers K, Hu YT, Verwer R, Balesar R, *et al*. MicroRNA-132 and early growth response-1 in nucleus basalis of Meynert during the course of Alzheimer's disease. Brain: a Journal of Neurology. 2016; 139: 908–921.

[38] Theriault FM, Nuthall HN, Dong Z, Lo R, Barnabe-Heider F, Miller FD, *et al*. Role for Runx1 in the proliferation and neuronal differentiation of selected progenitor cells in the mammalian nervous system. The Journal of Neuroscience: the Official Journal of the Society for Neuroscience. 2005; 25: 2050–2061.

[39] Tang X, Sun L, Jin X, Chen Y, Zhu H, Liang Y, *et al*. Runt-Related Transcription Factor 1 Regulates LPS-Induced Acute Lung Injury via NF-κB Signaling. American Journal of Respiratory Cell and Molecular Biology. 2017; 57: 174–183.

[40] Tripathi DM, Rohilla S, Kaur I, Siddiqui H, Rawal P, Juneja P, *et al*. Immunonano-Lipocarrier-Mediated Liver Sinusoidal Endothelial Cell-Specific RUNX1 Inhibition Impedes Immune Cell Infiltration and Hepatic Inflammation in Murine Model of NASH. International Journal of Molecular Sciences. 2021; 22: 8489.

[41] Logan TT, Villapol S, Symes AJ. TGF-β superfamily gene expression and induction of the Runx1 transcription factor in adult neurogenic regions after brain injury. PLoS ONE. 2013; 8: e59250.

[42] Yu M, Ou Y, Wang H, Gu W. PU.1 interaction with p50 promotes microglial-mediated inflammation in secondary spinal cord injury in SCI rats. The International Journal of Neuroscience. 2023; 133: 389–402.

[43] Huang KL, Marcora E, Pimenova AA, Di Narzo AF, Kapoor M, Jin SC, *et al*. A common haplotype lowers PU.1 expression in myeloid cells and delays onset of Alzheimer's disease. Nature Neuroscience. 2017; 20: 1052–1061.

[44] Pimenova AA, Herbinet M, Gupta I, Machlovi SI, Bowles KR, Marcora E, *et al*. Alzheimer's-associated PU.1 expression levels regulate microglial inflammatory response. Neurobiology of Disease. 2021; 148: 105217.

[45] Erdoğan Ö, Xie L, Wang L, Wu B, Kong Q, Wan Y, *et al*. Proteomic dissection of LPS-inducible, PHF8-dependent secretome reveals novel roles of PHF8 in TLR4-induced acute inflammation and T cell proliferation. Scientific Reports. 2016; 6: 24833.

[46] Chen X, Wang S, Zhou Y, Han Y, Li S, Xu Q, *et al*. Phf8 histone demethylase deficiency causes cognitive impairments through the mTOR pathway. Nature Communications. 2018; 9: 114.

[47] Strohmeyer R, Shelton J, Lougheed C, Breitkopf T. CCAAT-enhancer binding protein-β expression and elevation in Alzheimer's disease and microglial cell cultures. PLoS ONE. 2014; 9: e86617.

[48] Wang ZH, Xiang J, Liu X, Yu SP, Manfredsson FP, Sandoval IM, *et al*. Deficiency in BDNF/TrkB Neurotrophic Activity Stimulates δ-Secretase by Upregulating C/EBPβ in Alzheimer's Disease. Cell Reports. 2019; 28: 655–669.e5.

[49] Qin X, Wang Y, Paudel HK. Inhibition of Early Growth Response 1 in the Hippocampus Alleviates Neuropathology and Improves Cognition in an Alzheimer Model with Plaques and Tangles. The American Journal of Pathology. 2017; 187: 1828–1847.

[50] Yan SF, Fujita T, Lu J, Okada K, Shan Zou Y, Mackman N, *et al*. Egr-1, a master switch coordinating upregulation of divergent gene families underlying ischemic stress. Nature Medicine. 2000; 6: 1355–1361.

[51] Battle CE, Abdul-Rahim AH, Shenkin SD, Hewitt J, Quinn TJ. Cholinesterase inhibitors for vascular dementia and other vascular cognitive impairments: a network meta-analysis. The Cochrane Database of Systematic Reviews. 2021; 2: CD013306.

[52] Kavirajan H, Schneider LS. Efficacy and adverse effects of cholinesterase inhibitors and memantine in vascular dementia: a meta-analysis of randomised controlled trials. The Lancet. Neurology. 2007; 6: 782–792.

[53] Sung PS, Chen PW, Yen CJ, Shen MR, Chen CH, Tsai KJ, *et al*. Memantine Protects against Paclitaxel-Induced Cognitive Impairment through Modulation of Neurogenesis and Inflammation in Mice. Cancers. 2021; 13: 4177.

[54] Elbaz EM, Essam RM, Ahmed KA, Safwat MH. Donepezil halts acetic acid-induced experimental colitis in rats and its associated cognitive impairment through regulating inflammatory/oxidative/apoptotic cascades: An add-on to its anti-dementia activity. International Immunopharmacology. 2023; 116: 109841.

[55] Chen Y, Wang B, Liu D, Li JJ, Xue Y, Sakata K, *et al*. Hsp90 chaperone inhibitor 17-AAG attenuates Aβ-induced synaptic toxicity and memory impairment. The Journal of Neuroscience: the Official Journal of the Society for Neuroscience. 2014; 34: 2464–2470.

[56] Li J, Yang F, Guo J, Zhang R, Xing X, Qin X. 17-AAG post-treatment ameliorates memory impairment and hippocampal CA1 neuronal autophagic death induced by transient global cerebral ischemia. Brain Research. 2015; 1610: 80–88.

[57] Liao G, Khan M, Zhao Z, Arooj S, Yan M, Li X. Bevacizumab Treatment of Radiation-Induced Brain Necrosis: A Systematic Review. Frontiers in Oncology. 2021; 11: 593449.

[58] Xue R, Chen M, Cai J, Deng Z, Pan D, Liu X, *et al*. Blood-Brain Barrier Repair of Bevacizumab and Corticosteroid as Prediction of Clinical Improvement and Relapse Risk in Radiation-Induced Brain Necrosis: A Retrospective Observational Study. Frontiers in Oncology. 2021; 11: 720417.

[59] Kim ID, Cave JW, Cho S. Aflibercept, a VEGF (Vascular Endothelial Growth Factor)-Trap, Reduces Vascular Permeability and Stroke-Induced Brain Swelling in Obese Mice. Stroke. 2021; 52: 2637–2648.